Order Recursive Method of Moments (ORMoM) for Iterative Design Applications

Krishna Naishadham, *Member, IEEE*, and Pradeep Misra, *Member, IEEE*

Abstract— **The method of moments (MoM) continues to be the most frequently used full-wave electromagnetic simulation technique for application to CAD and optimization of microwave circuits. In this paper, we present an order-recursive variant of standard LU decomposition for the efficient solution of moderately large linear systems arising in the application of MoM to iterative design problems. In comparison with the existing solution methods suitable to matrices of size such that direct resolution of the linear systems by Gaussian elimination or LU decomposition becomes feasible, the proposed order-recursive MoM (ORMoM) allows a very large portion of repetitive computations (from scratch) at each design iteration to be avoided, leading to extremely efficient design cycles. Specifically, it is shown that ORMoM results in an order of magnitude reduction in the solution time for typical microwave design tasks. Therefore, this contribution is a major advance toward EM simulation-based CAD and optimization of microwave circuits.**

I. Introduction

INCREASING operating frequencies in digital and microwave systems have necessitated the utilization of full-wave electromagnetic (EM) simulation techniques, such as the method of moments (MoM) [1], the finite element method [2], and the finite-difference time-domain (FDTD) method [3], [4], for the analysis of high-speed digital circuits, microwave and millimeter-wave integrated circuits (MMIC's). These rigorous techniques account for physical phenomena such as surface-wave coupling, radiation, dispersion, metallization and dielectric losses. However, they are typically computation-intensive, and therefore, are of limited use in the computer-aided design (CAD) and optimization of microwave circuits. Therefore, it is desirable to investigate means of improving the efficiency of full-wave methods so that a circuit of moderate electrical size can be simulated in reasonable time on a personal computer (PC) or a workstation. These computer platforms, and not large-scale mainframes or supercomputers, seem to represent the typical design environment in the microwave industry.

The MoM is perhaps the most widely used EM simulation method for the analysis and CAD of microwave circuits. Several software houses offer commercial MoM-based simulation tools for the microwave circuit designer, e.g., [5]–[10]. These software packages have the capability to incorporate optimization features either internally [6], or by coupling the MoM simulation engine to an external parametrized optimizer [5], [10]. Several researchers are also investigating methods to improve the efficiency of MoM-based circuit simulators so that robust CAD tools and optimizers can be developed for the smaller computational platforms. These investigations include the application of wavelet transforms to sparsify the moment matrix [11], utilization of symmetries and redundancies in the problem space to efficiently fill the matrix [12], space mapping optimization techniques [13], application of order-recursive Gaussian elimination (ORGE) to resolve the linear systems [14], [15], and acceleration procedures for matrix-fill when small geometrical perturbations are involved in the design [16].

In the MoM, the boundary value problem for the unknown current distribution over the surface of the conductors is formulated as an electrical field integral equation (EFIE). The EFIE is then converted into a system of linear algebraic equations (for the current) by the minimization of weighted residuals using suitable basis and testing functions. Parameters of interest, such as S-parameters, radiation and metallization losses, can be derived from the computed current distribution. The current distribution can be computed by implementing the MoM algorithm either in the space domain (cf. [17]) or in the spectral domain (cf. [18]).

The system (or moment) matrix that represents the interactions between the basis and the test elements is typically dense. For moderately high-order models ($\mathcal{O}(100\text{–}500)$), the current distribution may be obtained as the solution of a system of linear algebraic equations using LU decomposition and subsequent solution of two triangular systems of equations. The computational complexity of solving a system of equations of order N is N^3. For several applications, where N is fixed, the use of conventional LU decomposition provides an efficient means for solving the linear systems.

However, in design applications, the order of the linear system to be solved may change from N to $N + M$, where the original $(N \times N)$ data matrix becomes a submatrix of the higher-order $(N + M) \times (N + M)$ matrix as a result of augmenting the model. This is frequently encountered, for example, in the tuning of patch antennas and microwave filters, where the data matrix is recursively augmented with new row and column vectors that correspond to shorting pins, stubs, etc. In a CAD environment, the order M of augmentation is usually not known *a priori*. At present, each augmented matrix is treated as a new data matrix and the solution of the augmented system of equations is recomputed from scratch. The resulting solution procedure becomes computationally inefficient, and, as shown elsewhere (see Section III), the computational complexity can become $\mathcal{O}((N + M)^4)$. The authors' previous investigations reveal that when small changes are made to the circuit geometry 1) they correspond

Manuscript received April 8, 1996.

The authors are with the Department of Electrical Engineering, Wright State University, Dayton, OH 45435 USA.

Publisher Item Identifier S 0018-9480(96)08548-1.

to changes in a small subsystem of the original linear system to be solved for the current distribution and 2) the solution for the current resulting from these small geometrical changes is only slightly perturbed from the prior solution [15]. The existing software packages with EM simulators based on the moment method do not seem to take advantage of the fact that most of the computations performed at a previous iteration can be embedded into the new system of algebraic equations. Instead, they remodel the entire system and solve the system so obtained from scratch, which is obviously not efficient, especially if direct solvers such as LU decomposition are employed. The objective of this paper is to apply an order-recursive variant of LU decomposition to develop a solution procedure which will allow a very large portion of the recomputation, necessitated by small perturbations of the geometry, to be avoided, leading to extremely efficient design iterations. The relative length scale over which the geometry is perturbed is assumed to be much smaller than (typically less than a tenth of) the characteristic wavelength at the maximum excitation frequency. This assumption is consistent with the observation that in microwave circuit optimization, usually small perturbation theory is employed in order to ensure stability and facilitate rapid convergence [19]. Therefore, this contribution is a major advance toward EM simulation-based (or full-wave) CAD and optimization of microwave circuits. The computational complexity of the proposed method is shown to be $\mathcal{O}((N+M)^3)$. Clearly, this order of magnitude reduction in computations is very attractive for interactive design tasks. It is pointed out that such reduction in operations count is exactly the same as that of ORGE [15]. However, as will be shown in Section III, the proposed order-recursive LU decomposition is simpler in implementation.

There are also situations encountered in design where one iteratively decreases the size or spacing of certain elements in a circuit or antenna geometry in order to meet the design specifications. Consider, for example, the reduction in stub length in the optimization of a monolithically loaded tunable patch antenna, or the reduction in width of a section of a microstrip quarter-wave transformer to compensate for dispersion. In these situations, the moment matrix is affected by removal of (or, is decremented by) certain row or column vectors associated with the changes in the circuit. As in augmented systems, the order of decrementation is not known *a priori*. At present, the solution of each decremented system of equations is recomputed from scratch. We propose an order-recursive solver for decremented MoM systems as well, wherein the solution (specifically, the LU-decomposition) at the prior iteration is used to efficiently solve the reduced system of equations at the present iteration. The application of efficient solvers for augmented and decremented systems to MoM results in a powerful technique, termed as the *order recursive method of moments* (ORMoM), with potential improvement in iterative design of complex structures using full-wave simulation.

The paper is organized as follows. In the next section, some preliminaries of the moment method implementation with regard to efficiencies in formulation and matrix-fill operation are discussed. In the subsequent section, the solution method for ORMoM is developed for both augmented and decremented systems. The operations count for ORMoM relative to the current method of resolving the linear system from scratch at each iteration is presented. Next, the computational efficiency of ORMoM is illustrated by applying it to three design problems. First, we consider the problem of determining the resonant size of a strip in free space by recursively constructing the solution for the current distribution on the strip as a function of varying strip size, with the frequency fixed. Secondly, we consider the tuning of monolithically stub-loaded dual-band patch antennas [20], which find application in mobile communications systems because of their light weight, low profile and ease of fabrication. It is well-known that rectangular microstrip patch antennas with reactive stubs placed along the radiating edges exhibit dual frequency operation [20], [21]. Finally, we iteratively "fine-tune" the design of a folded double-stub microstrip filter to achieve the desired specifications in the pass-band for the insertion loss. At each iteration, either the spacing between, or the length of the stubs, is varied (incremented or decremented), as would be typically required in a circuit optimization environment, and the modified system of equations is solved efficiently for the current distribution by using order recursion. Favorable comparison of these simulated data with published or measured results serves to validate the computations. More importantly, these design applications of ORMoM are anticipated to highlight the capability of the proposed method to improve the computational efficiency of full-wave design of MMIC's of arbitrary geometrical complexity.

II. Order Recursive Method of Moments

A. Outline of MoM Formulation

In MoM, the boundary value problem for the current distribution on the surface of a conductor is formulated as an EFIE, which states that the total tangential electric field on a perfect electrically conducting (PEC) surface is zero

$$-\boldsymbol{E}_t^{\text{scat}}(\boldsymbol{r}) = \boldsymbol{E}_t^{\text{inc}}(\boldsymbol{r}), \qquad \boldsymbol{r} \in S_c \tag{1}$$

where S_c denotes the conductor surface, the subscript t denotes the tangential component, and $\boldsymbol{r}$ is the position vector to the observation point. The scattered field is given by

$$\boldsymbol{E}_t^{\text{scat}}(\boldsymbol{r}) = \int_{S_c} \overline{\overline{\boldsymbol{G}}}_E(\boldsymbol{r}, \boldsymbol{r}') \cdot \boldsymbol{J}_S(\boldsymbol{r}')\, ds' \tag{2}$$

where $\overline{\overline{\boldsymbol{G}}}_E$ is the appropriate transverse part of the electric field dyadic Green's function and can be obtained in terms of scalar and vector potentials involving Sommerfeld integrals [17]. The incident field is defined to be the field existing in the absence of the scattering object. It simply equals the field impressed on S_c by a known excitation source. The current $\boldsymbol{J}_S$ can be expanded in terms of sub-sectional basis elements as

$$\boldsymbol{J}_S(\boldsymbol{r}') \approx \sum_{n=1}^{N} I_n \boldsymbol{f}_n(\boldsymbol{r}'). \tag{3}$$

After substituting (3) in (2) and testing the resulting equation with identical basis elements (Galerkin method), we obtain

the linear system of equations

$$\begin{bmatrix} \boldsymbol{Z}^{xx} & \boldsymbol{Z}^{xy} \\ \boldsymbol{Z}^{yx} & \boldsymbol{Z}^{yy} \end{bmatrix} \begin{bmatrix} \boldsymbol{I}_x \\ \boldsymbol{I}_y \end{bmatrix} = \begin{bmatrix} \boldsymbol{V}^i \\ \boldsymbol{0} \end{bmatrix} \tag{4}$$

where an incident field given by delta-gap voltage excitation at a finite number of ports, M, is assumed [22], [23]

$$\boldsymbol{E}_t^{\text{inc}}(\boldsymbol{r}) = \sum_{k=1}^{M} V_k^i \delta(\boldsymbol{r} - \boldsymbol{r}_k)\boldsymbol{a}_{tk}. \tag{5}$$

In (5), V_k^i denotes the amplitude of the impressed voltage, the position vector $\boldsymbol{r}_k$ locates the port k, and $\boldsymbol{a}_{tk}$ is the outward unit vector tangential to the kth feed-line. The linear system in (4) is solved for the transverse currents $[I_x]$ and $[I_y]$. Network parameters pertinent to characterization of the microwave circuit, such as S-parameters, can be directly obtained from the computed currents (cf. [17]). We have used roof-top basis elements [17] for expansion and testing. The matrix elements in (4) can be computed as

$$Z_{mn}^{pq} = \int_{S_c}\int_{S_c} f_{mp}(\boldsymbol{r}) G_{E,pq}(\boldsymbol{r},\boldsymbol{r}') f_{nq}(\boldsymbol{r}')\, ds'\, ds \tag{6}$$

where $p = x$ or y (the conducting surface is assumed to lie in the xy-plane), and $G_{E,pq} = \boldsymbol{a}_p \cdot \overline{\overline{\boldsymbol{G}}}_E \cdot \boldsymbol{a}_q$.

B. Efficient Computation of the Moment Matrix

In order to examine the pressing need for efficient computation of the moment matrix in design applications, let us reconsider (1) at the first design iteration (henceforth, the iteration number will be denoted by a superscript)

$$-\int_{S_c^1} \overline{\overline{\boldsymbol{G}}}_E(\boldsymbol{r},\boldsymbol{r}') \cdot \boldsymbol{J}_S(\boldsymbol{r}')\, ds' = \boldsymbol{E}_t^{\text{inc}}(\boldsymbol{r}), \qquad \boldsymbol{r} \in S_c^1 \tag{7}$$

with

$$\boldsymbol{r} = \boldsymbol{a}_x x + \boldsymbol{a}_y y, \quad \boldsymbol{r}' = \boldsymbol{a}_x x' + \boldsymbol{a}_y y'$$

and S_c^1 is the conducting surface support for the first iteration on which currents need to be computed. In matrix form, assuming a single delta-gap voltage source at $\boldsymbol{r} = \boldsymbol{r}_k$ for simplicity, we have

$$\sum_{n=1}^{N^{(1)}} Z_{mn} I_n = V_m^i \delta_{mk}, \quad \delta_{mk} = \begin{cases} 1, & k = m \\ 0, & \text{otherwise} \end{cases} \tag{8}$$

for $m = 1, 2, \cdots, N^{(1)}, k \in [1, M]$. $N^{(i)}$ is the number of basis elements used at the ith iteration and

$$Z_{mn} = \int_{S_c^1}\int_{S_c^1} \boldsymbol{f}_m(\boldsymbol{r}) \cdot \overline{\overline{\boldsymbol{G}}}_E(\boldsymbol{r},\boldsymbol{r}') \cdot \boldsymbol{f}_n(\boldsymbol{r}')\, ds'\, ds. \tag{9}$$

It is evident that the number of basis elements is proportional to the size of the conducting surface support for a given accuracy. Now, suppose that during the second iteration, the size of the object is increased from S_c^1 to $S_c^2 = S_c^1 + \Delta S_c$. Let the corresponding increase in the number of basis elements be ΔN. With $N^{(2)} = N^{(1)} + \Delta N$, we now have

$$\sum_{n=1}^{N^{(2)}} Z_{mn} I_n = V_m^i \delta_{mk}, \qquad m = 1, 2, \cdots, N^{(1)}, \\ [N^{(1)} + 1], \cdots, N^{(2)} \tag{10}$$

$$Z_{mn} = \int_{S_c^2}\int_{S_c^2} \boldsymbol{f}_m(\boldsymbol{r}) \cdot \overline{\overline{\boldsymbol{G}}}_E(\boldsymbol{r},\boldsymbol{r}') \cdot \boldsymbol{f}_n(\boldsymbol{r}')\, ds'\, ds. \tag{11}$$

If the support of the first $N^{(1)}$ basis elements is unchanged, one need not recompute $Z_{mn}, m = 1, 2, \cdots, N^{(1)}; n = 1, 2, \cdots, N^{(1)}$ in (11). This can be seen more clearly by rewriting (11) using linear superposition as

$$Z_{mn} = \left(\int_{S_c^1} + \int_{\Delta S_c}\right) g_{mn}(\boldsymbol{r})\, ds$$

$$g_{mn}(\boldsymbol{r}) = \left(\int_{S_c^1} + \int_{\Delta S_c}\right) \boldsymbol{f}_m(\boldsymbol{r}) \cdot \overline{\overline{\boldsymbol{G}}}_E(\boldsymbol{r},\boldsymbol{r}') \cdot \boldsymbol{f}_n(\boldsymbol{r}')\, ds'. \tag{12}$$

In other words, when the physical size of the circuit is increased from S_c^1 to S_c^2, provided that the discretization is unchanged on that part of the circuit geometry which is retained from prior iterations, one need not recompute the moment integrals already computed in these iterations. For the subsequent iterations, we need to evaluate only those integrals which arise from the reactions associated with expansion and test elements placed on the circuit (or surface) extension, ΔS_c. In matrix form, we arrive at a bordered system of equations given by

$$\left[\begin{array}{cc|cc} \boldsymbol{Z}_{xx}^{11} & \boldsymbol{Z}_{xy}^{11} & \boldsymbol{Z}_{xx}^{12} & \boldsymbol{Z}_{xy}^{12} \\ \boldsymbol{Z}_{yx}^{11} & \boldsymbol{Z}_{yy}^{11} & \boldsymbol{Z}_{yx}^{12} & \boldsymbol{Z}_{yy}^{12} \\ \hline \boldsymbol{Z}_{xx}^{21} & \boldsymbol{Z}_{xy}^{21} & \boldsymbol{Z}_{xx}^{22} & \boldsymbol{Z}_{xy}^{22} \\ \boldsymbol{Z}_{yx}^{21} & \boldsymbol{Z}_{yy}^{21} & \boldsymbol{Z}_{yx}^{22} & \boldsymbol{Z}_{yy}^{22} \end{array}\right] \left[\begin{array}{c} \boldsymbol{I}_x^1 \\ \boldsymbol{I}_y^1 \\ \hline \boldsymbol{I}_x^2 \\ \boldsymbol{I}_y^2 \end{array}\right] = [\boldsymbol{V}]$$

$$\begin{bmatrix} \boldsymbol{Z}^{11} & \boldsymbol{Z}^{12} \\ \boldsymbol{Z}^{21} & \boldsymbol{Z}^{22} \end{bmatrix} \begin{bmatrix} \boldsymbol{I}^1 \\ \boldsymbol{I}^2 \end{bmatrix} = [\boldsymbol{V}] \tag{13}$$

where the second superscript of each submatrix indicates the iteration corresponding to location of the current expansion element, while the first indicates that corresponding to the test element location. For example, with the cells numbered sequentially from iteration to iteration, $\boldsymbol{Z}_{xy}^{12}$ represents the reaction between a y-directed basis element along the circuit extension (or second iteration) and a test element on the surface support considered in the first iteration. The submatrices calculated in the prior iterations are unchanged in subsequent iterations. Normally, for each subsequent design iteration, the number of rows and columns added to the moment matrix is small in comparison with its existing size. This is because the geometrical size, e.g., length of the tuning stubs in a filter, is changed by a small increment at each step in CAD and optimization of microwave circuits. Alternatively, it is logical to assume that at any given design iteration, the circuit geometry is perturbed by small electrical dimensions relative to some significant portion of the circuit, whose geometry

remains unchanged. The above discussion can be generalized to any number of iterations, yielding

$$\begin{bmatrix} \boldsymbol{Z}^{11} & \boldsymbol{Z}^{12} & \cdots & \boldsymbol{Z}^{1m} & \cdots & \boldsymbol{Z}^{1M} \\ \boldsymbol{Z}^{21} & \boldsymbol{Z}^{22} & \cdots & \boldsymbol{Z}^{2m} & \cdots & \boldsymbol{Z}^{2M} \\ \vdots & \vdots & \ddots & \vdots & \ddots & \vdots \\ \boldsymbol{Z}^{M1} & \boldsymbol{Z}^{M2} & \cdots & \boldsymbol{Z}^{Mm} & \cdots & \boldsymbol{Z}^{MM} \end{bmatrix} \begin{bmatrix} \boldsymbol{I}^1 \\ \boldsymbol{I}^2 \\ \vdots \\ \boldsymbol{I}^M \end{bmatrix} = [\boldsymbol{V}] \tag{14}$$

where each submatrix has the interpretation in terms of x- and y-directed testing as shown in (13). The linear system in (14) is referred to as the augmented moment matrix model at the Mth design iteration [15]. Further design iterations create additional rows and columns at the border.

If metallization is removed from the circuit in a design application, then the moment matrix at the previous iteration is *decremented* by row and column vectors corresponding to the expansion and testing elements in the removed part. By block permutation of the removed rows and columns, the decremented matrix can again be arranged in a bordered form similar to (14) (see Section III). Further efficiency features are built into the MoM algorithm, such as exploitation of symmetries and redundancies for equal cell size [12], and moment matrix spatial and frequency interpolation [25].

The above discussion pertained primarily to efficient computation of the matrix elements to achieve computational savings in the matrix-fill operation. In the next section, we address how a solution method can be developed, which does not require the resolution of linear system of equations at each iteration from scratch. Instead, the solution at the prior iterations can be used to efficiently solve the system at the current iteration.

III. Order Recursive LU Decomposition

The proposed algorithm assumes that *all* the leading principal submatrices of the system (or moment) matrix $\boldsymbol{A}$ are nonsingular. Therefore, the solution (albeit suboptimal) can always be computed without the need of pivoting. Note that in the sequel, when computing LU decomposition, we refer to Crout reduction (1's along the diagonal of upper triangular matrix U). Identical results may be stated for Doolittle reduction (1's along the diagonal of lower triangular matrix L).

A. Augmented Systems

Assume that the LU decomposition of A $(= LU)$ has been computed. Denote an augmented matrix and its LU decomposition as

$$A := \left[\begin{array}{c|c} A_{11} & \boldsymbol{a}_{12} \\ \hline \boldsymbol{a}_{21} & a_{22} \end{array}\right] = \left[\begin{array}{c|c} L_{11} & \boldsymbol{o} \\ \hline \boldsymbol{l}_{21} & l_{22} \end{array}\right] \left[\begin{array}{c|c} U_{11} & \boldsymbol{u}_{12} \\ \hline \boldsymbol{o} & 1 \end{array}\right]. \tag{15}$$

Then, it is readily seen that the unknowns may be computed as

$$\begin{aligned} \boldsymbol{u}_{12} &= L_{11}^{-1}\boldsymbol{a}_{12} \\ \boldsymbol{l}_{21} &= \boldsymbol{a}_{21}U_{11}^{-1} \\ l_{22} &= a_{22} - \boldsymbol{l}_{21}\boldsymbol{u}_{12}. \end{aligned} \tag{16}$$

Of course one *must not* compute the inverses of matrices as shown in (16). Instead, the unknowns are obtained by solution of the triangular system of equations, which is known to be numerically stable. The above result is easily extended to the case when the matrix is bordered by several rows and columns. Specifically, if

$$A := \left[\begin{array}{c|c} A_{11} & A_{12} \\ \hline A_{21} & A_{22} \end{array}\right] = \left[\begin{array}{c|c} L_{11} & O \\ \hline L_{21} & L_{22} \end{array}\right] \left[\begin{array}{c|c} U_{11} & U_{12} \\ \hline O & U_{22} \end{array}\right] \tag{17}$$

then, the unknowns may be computed as

$$\begin{aligned} U_{12} &= L_{11}^{-1}A_{12} \\ L_{21} &= A_{21}U_{11}^{-1} \\ L_{22}U_{22} &:= A_{22} - L_{21}U_{12} \end{aligned} \tag{18}$$

where, the last equation in (18) represents an LU decomposition of the matrix on its right-hand side.

B. Decremented Systems

We have developed a similar approach for solving **decremented** moment systems, which pertains to the *removal* of certain elements or metallization in a structure. This situation is encountered, for example, when the stub length or separation in a microstrip filter needs to be decreased iteratively. In this case, the order of the new matrix is smaller than that of the original matrix. Specifically, we consider the update of LU decomposition of a matrix some of whose rows and columns are removed. It is, of course, assumed that the LU decomposition of the original *higher* order matrix is available. Consider the following (3×3) block matrix

$$A = \begin{bmatrix} A_{11} & A_{12} & A_{13} \\ A_{21} & A_{22} & A_{23} \\ A_{31} & A_{32} & A_{33} \end{bmatrix} = \begin{bmatrix} L_{11} & O & O \\ L_{21} & L_{22} & O \\ L_{31} & L_{32} & A_{33} \end{bmatrix} \begin{bmatrix} U_{11} & U_{12} & U_{13} \\ O & U_{22} & U_{23} \\ O & O & U_{33} \end{bmatrix}. \tag{19}$$

To see the effect of decrementing the matrix order by removing some rows and columns, it is instructive to consider the (block) LU decomposition of the matrix. Assuming that $A_{11} = L_{11}U_{11}$ is known, the remaining entries of the decomposition may be computed as follows:

$$\begin{aligned} U_{12} &= L_{11}^{-1}A_{12} \\ L_{21} &= A_{21}U_{11}^{-1} \\ L_{22}U_{22} &:= A_{22} - L_{21}U_{12} \end{aligned} \tag{20}$$

$$\begin{aligned} U_{13} &= L_{11}^{-1}A_{13} \\ L_{31} &= A_{31}U_{11}^{-1} \\ U_{23} &= L_{22}^{-1}(A_{23} - L_{21}U_{13}) \\ L_{32} &= (A_{32} - L_{31}U_{12})U_{22}^{-1} \\ L_{33}U_{33} &:= A_{33} - L_{31}U_{13} - L_{32}U_{23} \end{aligned} \tag{21}$$

where (20) and (21) represent LU decomposition of the matrix on the right-hand side.

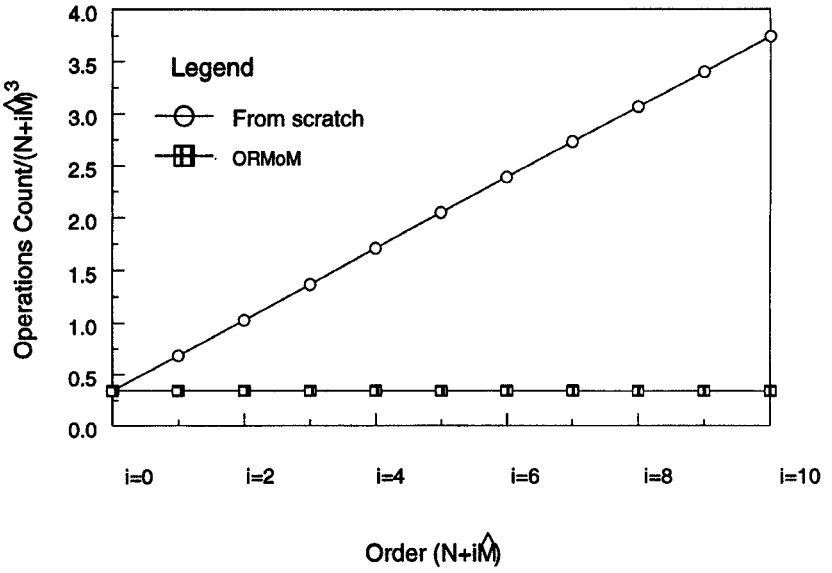

Fig. 1. Order of magnitude estimate of operations count.

The following three possibilities for deletion of block rows and columns exist. Irrespective of which rows and columns are deleted at a given iteration, by appropriate permutation of these row and column vectors, the moment matrix can always be arranged to correspond to one of the three bordered forms derived below.

Case 1: Delete (1, 1) Block Row and Column: In this case, the entire LU decomposition of the decremented matrix

$$A := \left[\begin{array}{c|cc} A_{11} & A_{12} & A_{13} \\ \hline A_{21} & A_{22} & A_{23} \\ A_{31} & A_{32} & A_{33} \end{array}\right] \rightarrow \begin{bmatrix} A_{22} & A_{23} \\ A_{32} & A_{33} \end{bmatrix}$$

must be recomputed. This is evident from the dependence of the entire decomposition on the LU decomposition of A_{11}.

Case 2: Delete (2, 2) Block Row and Column:

$$A := \left[\begin{array}{c|c|c} A_{11} & A_{12} & A_{13} \\ \hline A_{21} & A_{22} & A_{23} \\ \hline A_{31} & A_{32} & A_{33} \end{array}\right] \rightarrow \begin{bmatrix} A_{11} & A_{13} \\ A_{31} & A_{33} \end{bmatrix}$$

Following the operations described in (19)–(21) for recursive LU decomposition, it is seen that if

$$\begin{bmatrix} A_{11} & A_{13} \\ A_{31} & A_{33} \end{bmatrix} = \begin{bmatrix} L_{11}^{\text{new}} & O \\ L_{21}^{\text{new}} & L_{22}^{\text{new}} \end{bmatrix} \begin{bmatrix} U_{11}^{\text{new}} & U_{12}^{\text{new}} \\ O & U_{22}^{\text{new}} \end{bmatrix}$$

then, the matrices $L_{11}^{\text{new}}, L_{21}^{\text{new}}, U_{11}^{\text{new}}$ and U_{12}^{new} are the same as the matrices L_{11}, L_{31}, U_{11} and U_{13}, respectively. Hence they need not be recomputed. However, L_{22}^{new} and U_{22}^{new} are obtained from the LU decomposition of the original matrices $A_{33} - L_{31}U_{13}$ and need to be recomputed.

Case 3: Delete (3, 3) Block Row and Column:

$$A := \left[\begin{array}{cc|c} A_{11} & A_{12} & A_{13} \\ A_{21} & A_{22} & A_{23} \\ \hline A_{31} & A_{32} & A_{33} \end{array}\right] \rightarrow \begin{bmatrix} A_{11} & A_{12} \\ A_{21} & A_{22} \end{bmatrix}.$$

Again referring to the relations in recursive decomposition, it is easily seen that for this case, no new computations are required since the LU decomposition of the first (2×2) block submatrix is independent of the third (block) row and column.

C. Computational Complexity

It is clear from the description earlier in Section III that the computational complexity of ORMoM is identical to Gaussian elimination or conventional LU decomposition. The only difference is the sequence in which the elimination or decomposition is performed at each iteration. We will show next that the LU triangularization and back substitution together require in ORMoM $\mathcal{O}(N+M)^3$ operations, where $(N+M)$ is the dimension of the final augmented matrix. This reduction in operations count is irrespective of whether order-recursive Gaussian elimination [15] or LU decomposition is employed. Without any loss of generality, we consider the complexity of only augmented systems. If a new decomposition together with back substitution is performed for each system of order $(N+i\hat{M})$, where $i = 0, \cdots, r$ denotes the iteration number, $\hat{M}$ is the number of rows and columns by which the matrix is augmented in each iteration and $(r\hat{M}) = M$, then the operations count is approximately $\Sigma_{i=0}^{r}(N+i\hat{M})^3$. To see that the latter is an order of magnitude higher than the former $(\mathcal{O}(N+M)^3)$, consider the following example.

Let $N = 100, M = 10, r = 10$, i.e., we are augmenting the system matrix by ten rows and columns in each iteration and performing a total of ten iterations. The resulting operations count is shown in Fig. 1. Note that since the intent is to observe the order of magnitude complexity, the operations count has been weighted down by $(N+i\hat{M})^3$ for both methods at each iteration. It can be seen clearly that while the operations count of ORMoM exhibits a slope of zero (implying $\mathcal{O}(N+M)^3$ operations), as anticipated, the normalized count for the case when the entire solution is recomputed from scratch shows constant nonzero slope (implying $\mathcal{O}(N+M)^4$). It is evident

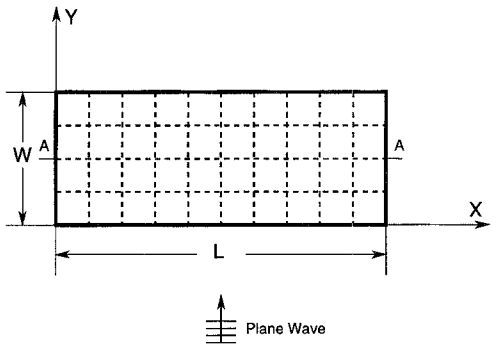

Fig. 2. A rectangular strip in free space with plane wave excitation.

that the computational savings of ORMoM are most significant when the iteration count is large.

IV. Design Examples

A. Resonant Size of a Strip

We consider the problem of recursively determining the current distribution on a rectangular strip in free space, shown in Fig. 2, in order to find its resonant size. It should be stated that the example is quite straightforward, and, as such, may be solved using direct LU decomposition. The intent here is to show how the problem may be cast in the ORMoM framework, and then, to verify that indeed the solution so obtained is accurate. The real impact of ORMoM will be seen on considerably higher-order problems.

The strip has dimensions $L = 0.5$ mm and $W = 0.2$ mm. The current distribution over the strip is computed by the MoM using roof-top basis functions and razor testing [17]. However, instead of directly solving for the current over a strip of size 0.5 mm $\times$ 0.2 mm, we employ ORMoM to recursively build this solution starting from a 0.2 mm $\times$ 0.2 mm strip and uniformly incrementing L in 3 iterations to 0.5 mm (W remains unchanged at 0.2 mm). In each iteration, the strip is divided into an appropriate number of square cells, each of side 0.05 mm. Because the resonant frequency is independent of the excitation, we consider a normally incident TM plane wave excitation (see Fig. 2). Let M and N denote the number of cells along x and y, respectively, while N_x and N_y denote the number of corresponding basis functions. Table I displays the order of the moment matrix, namely, $N_x + N_y$, at each iteration of ORMoM.

Fig. 3 displays the real and imaginary parts of the x-directed current along the AA-cut (see Fig. 2) through the center of the strip. The current location is measured by the cell number. The wavelength of excitation is 1 mm. As discussed earlier, the strip size is successively extended along the x-direction by two cells at each iteration, starting from a length of four cells. The cell numbers along the x-direction at each iteration are shown in the first column of Table I. Four cells are maintained constantly along the y-direction. The curve in Fig. 3 for abscissa between zero and four corresponds to the first iteration, that between zero and six corresponds to the second, and so on. The current at each iteration has been computed efficiently using the decomposition at the previous iteration.

TABLE I
Order of Matrices for Different Strip Dimensions

M	N	N_x	N_y	Order
4	4	12	12	24
6	4	20	18	38
8	4	28	24	52
10	4	36	30	66

The complex current in the last iteration has been compared to the direct MoM computation from [17]. It has been found that the two results agree within eight decimal places for both real and imaginary currents. A similar validation has been observed for the y-directed current also, but, it is not presented for brevity. We believe that the accurate calculation of surface current distribution is a much more stringent test of validation than comparisons based on far-field parameters or circuit parameters. All these parameters are ultimately computed using the current distribution determined by the MoM. Simulation of the same example using ORGE instead of LU decomposition to determine the current distribution gave identical results [15], reinforcing the confidence in results produced by either method.

It is observed from Fig. 3 that the imaginary part of the current changes sign between the third and the fourth iterations. Hence, the resonant size of the strip lies between $L = 8$ cells and $L = 10$ cells. The theoretical resonant size is defined as the value of L for which the imaginary part of the current is zero. However, computationally, the imaginary part goes through a minimum (within a prescribed numerical tolerance set by the floating point architecture of the computer) at the *real* frequency at which the determinant of the moment matrix has a local minimum. Because of radiation, the theoretical resonant frequency is actually *complex*, and it defines most accurately the resonant condition that the imaginary current is zero [26]. We performed a fifth iteration wherein L is decreased form ten to nine cells, and found that the magnitude of the imaginary current distribution is indeed small (of the order of 10^{-4}) over the entire strip. A lower current magnitude can be obtained by further fine-tuning L around $L = 9$ cells. This may not, however, be warranted by the physical dimensional tolerances set in practice. When the length of the strip is reduced from 10 cells to 9 cells, ORMoM for decremented systems has been employed for the solution of the current. It is emphasized that we have not performed any search of the minimum of the determinant to find the resonant frequency. This search operation is itself quite expensive computationally, and is very unstable in view of the singular nature of the moment matrix around a resonant frequency.

A few important conclusions may be inferred from this simulation. First, ORMoM provides an efficient means of accurately determining the approximate neighborhood of the resonant frequency (or size). Second, some characteristic geometrical attribute which predominantly influences the resonance (such as L in this example) may be sub-gridded into smaller cells, and ORMoM can be applied to efficiently compute the current distribution for the new geometry in

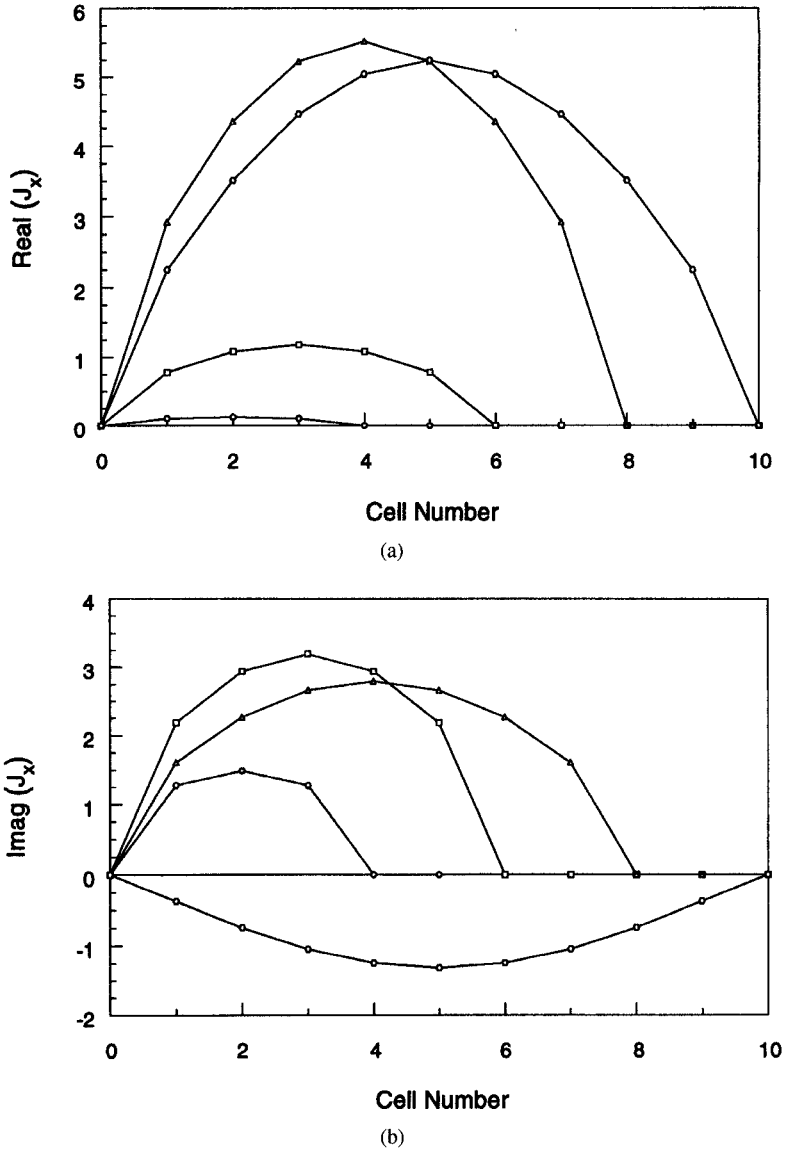

Fig. 3. Current distribution along AA cut: (a) real current and (b) imaginary current.

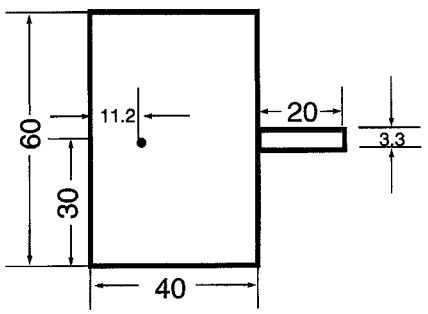

Fig. 4. Patch antenna geometry (all dimensions in mm).

terms of the solution at the previous iteration. Third, a simple optimization procedure, such as the bisection algorithm, can be combined with ORMoM to accurately track the zero of the imaginary current (or some such performance attribute) from a very good initial guess of the strip size provided by the preliminary iterations. While these aspects of ORMoM are very attractive to optimization of microwave circuits, further studies need to be conducted to determine the stability of ORMoM in the vicinity of the resonance. A MoM algorithm which accomodates unequal cell sizes and a mixture of different cell shapes (e.g., triangular and rectangular patches [27]) appears to be best-suited for incorporation of the optimizer in ORMoM.

B. Dual Band Patch Antenna

The solution procedure described in Section III is applied to the iterative design of a coax-fed tunable dual-band patch antenna, whose geometry is shown in Fig. 4. The substrate is 0.79 mm thick duroid ($\epsilon_r = 2.17$). The patch and the stub are gridded into a rectangular mesh which supports rooftop basis functions. The resulting moment matrix for the patch alone is of the order 216. The return loss of the untuned patch is shown in Fig. 5 and a fundamental resonance is observed at

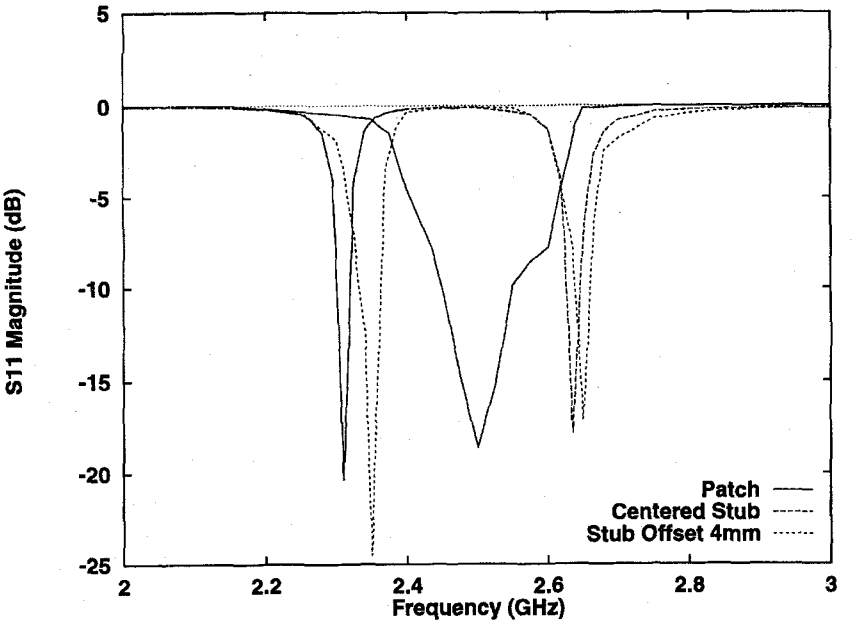

Fig. 5. Return loss of the tuned patch antenna.

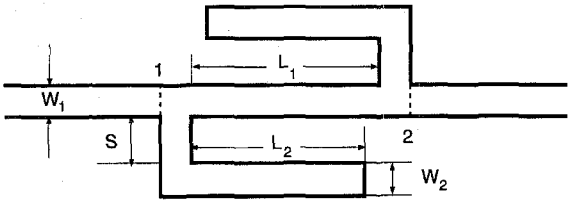

Fig. 6. Microstrip double folded-stub filter.

2.5 GHz. In order to provide dual-band operation, an open-circuited $\lambda/4$ monolithic stub is connected perpendicular to a radiating edge (Fig. 4) and its position along the edge or its length is varied iteratively. At each iteration, instead of solving the linear system of moment equations from scratch, the LU decomposition of the patch is efficiently utilized in solving the augmented system created by the addition of the stub.

Two positions of the 20 mm long stub are simulated: a) center of the radiating edge, b) 4 mm above the center. In either case, the 216 × 216 system matrix of the patch is augmented by 8 rows and columns. Location a) produces two resonances at 2.31 and 2.635 GHz (Fig. 5) in contrast to the experimentally observed values, 2.275 and 2.666 GHz, respectively [20]. The separation of the resonances can be varied by moving the stub along the radiating edge. Location b) produces the resonances at 2.35 and 2.65 GHz (Fig. 5), clearly demonstrating the tuning nature of the stub. Because of symmetry, a similar band separation has been observed when the stub is located 4 mm below the center of the radiating edge.

As an indication of computational efficiency of ORMoM, the conventional MoM implementation of solving the currents from scratch at each iteration would have required $216^3 + 224^3 = 21\,317\,120$ operations, whereas ORMoM requires only $216^3 + 2 \times 8 \times 216^2 = 10\,824\,192$ operations (savings of about

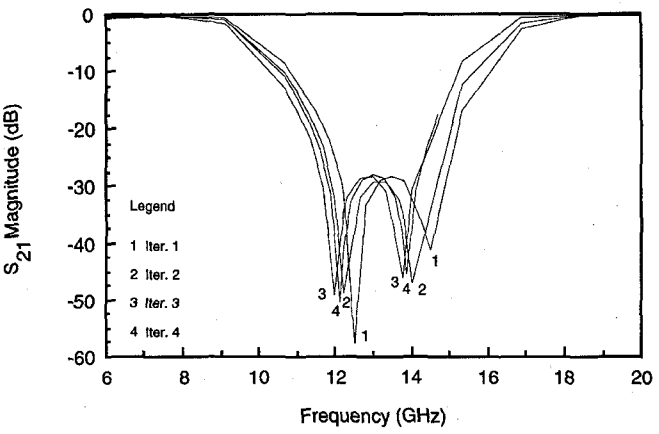

(a)

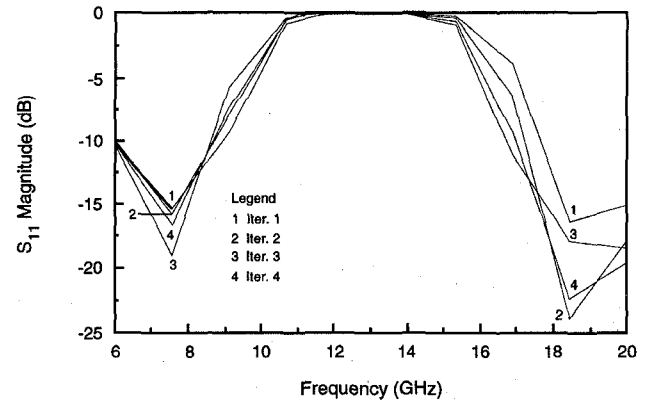

(b)

Fig. 7. Iterative double folded-stub filter design: (a) $|S_{21}|$, (b) $|S_{11}|$.

TABLE II
PARAMETERS FOR ITERATIVE DESIGN OF THE FOLDED-STUB FILTER

Iter.	L_1	L_2	S
1	90	80	4.8
2	91.5	85.7	4.1
3	93.7	85.3	4.6
4	92.1	85.1	4.2

50%). It is evident that the computational savings would be larger for higher-order problems, and for those involving many iterations (e.g., in optimization).

C. Folded-Stub Microstrip Filter

Next, we consider the design of a folded double-stub microstrip filter seen in Fig. 7 with design specifications given by [13]

$$|S_{21}| \geq -3\,\text{dB}, \quad \begin{cases} f \leq 9.5\,\text{GHz} \\ f \geq 16.5\,\text{GHz} \end{cases}$$

$$|S_{21}| \leq -30\,\text{dB}, \quad \begin{cases} f \leq 14\,\text{GHz} \\ f \geq 12\,\text{GHz}. \end{cases}$$

The substrate has a thickness of 5 mils and $\epsilon_r = 9.9$. The two stubs have the same width as the main line, given by $W_1 = W_2 = 4.8$ mils, and equal length. The parameters L_1, L_2 and S are varied iteratively as shown in Table II, and the performance of the filter is evaluated in terms of the insertion loss at each iteration until the design specifications are met. Note that changing L_1 alters the horizontal spacing between the stubs, whereas changing L_2 varies the length of the stubs. Variation of S affects the vertical spacing between the stubs. The three designable parameters are either incremented or decremented at each iteration following the entries in Table II, and ORMoM is employed to efficiently compute the current distribution.

The insertion loss (magnitude of S_{21} in dB) and return loss (magnitude of S_{11} in dB) of the filter are plotted in Fig. 7. The design in first iteration does not meet the specifications on insertion loss at several frequencies in the 12 to 14 GHz band. Also, both of the notches are quite discrepant from the optimized solutions of approximately 12 GHz and 14 GHz [13]. The subsequent iterations are observed to improve the insertion loss toward the specifications, with the fourth iteration yielding a response close to the best-optimized fine model simulation in Fig. 9 of [13]. In a frequency band of approximately 0.5 GHz around 13 GHz, the insertion loss for all the iterations is offset from the design specification of -30 dB by about 2 dB. This is perhaps within the numerical accuracy of the moment method implementation used in either investigation. The return loss shown in Fig. 7 is nominally less than -10 dB in each passband away from the central notch of 13 GHz, and clearly demonstrates the band-reject nature of the filter.

V. CONCLUSION

An order-recursive variant of conventional LU decomposition has been presented for the efficient solution of linear systems arising in an iterative moment method simulation, with potential application to microwave CAD and optimization. The method is illustrated by interactive design of a tunable dual-band microstrip patch antenna and a microstrip band-reject filter. The application of ORMoM to determine the characteristic resonant dimensions of a strip in free space shows that ORMoM has significant potential in microwave circuit optimization. We are currently investigating the application of ORMoM to improve solution accuracy and numerical resolution of the simulation by increasing the cell density in regions of high field variation, keeping lower density in others, where no such variation exists. The goal is to provide an efficient full-wave analysis tool for EM optimization, which does not have the serious limitation [13] of having the same cell size in all computational regions.

REFERENCES

[1] R. F. Harrington, *Field Computation by Moment Methods*. New York: Macmillan, 1968.
[2] J. Jin, *The Finite Element Method in Electromagnetics*. New York: Wiley, 1992.
[3] K. S. Kunz and R. J. Luebbers, *The Finite Difference Time Domain Method for Electromagnetics*. Boca Raton, FL: CRC Press, 1993.
[4] A. Taflove, *Computational Electrodynamics: The Finite-Difference Time-Domain Method*. Norwood, MA: Artech House, 1995.
[5] *em*, Sonnet Software, Liverpool, NY 13090.
[6] *IE3D*, Zeland Software, Inc., Fremont, CA 94538.
[7] *Ensemble*, Boulder Microwave Technologies, Inc., Boulder, CO 80302.
[8] *Explorer*, Compact Software, Paterson, NJ 07504.
[9] *Momentum EM Simulator*, Hewlett–Packard, Westlake Village, CA 91362.
[10] *OSA90/hope* and *EMpipe*, Optimization Systems Associates, Inc., Dundas, Ontario, Canada.
[11] K. Sabetfakhri and L. P. B. Katehi, "Analysis of integrated millimeter-wave and submillimeter-wave waveguides using orthonormal wavelet expansions," *IEEE Trans. Microwave Theory Tech.*, vol. 42, pp. 2412–2422, Dec. 1994.
[12] K. Naishadham and T. W. Nuteson, "Efficient analysis of passive microstrip elements in MMICs," *Int. J. Microwave Millimeter-Wave Comp. Aided Eng.*, vol. 4, no. 3, pp. 219–229, 1994.
[13] J. Bandler *et al.*, "Space mapping technique for electromagnetic optimization," *IEEE Trans. Microwave Theory Tech.*, vol. 42, pp. 2536–2544, Dec. 1994.
[14] K. Naishadham and P. Misra, "Order recursive Gaussian elimination and efficient CAD of microwave circuits," in *IEEE Microwave Symp. Dig.*, May 1995, pp. 1435–1438.
[15] P. Misra and K. Naishadham, "Order recursive Gaussian elimination (ORGE) and efficient CAD of microwave circuits," *IEEE Trans. Microwave Theory Tech.*, vol. 44, no. 12, pp. 2166–2173, Dec. 1996.
[16] G. P. Junker, A. A. Kishk, and A. W. Glisson, "Rapid parametric study of antennas using method of moments" *Annual Review of Progress in Applied Computational Electromagnetics*, vol. 2, pp. 784–791, Mar. 1996.
[17] J. R. Mosig, "Integral Equation Technique," in *Numerical Techniques for Microwave and Millimeter-Wave Passive Structures*, T. Itoh, ed. New York: Wiley, 1989, pp. 133–213.
[18] R. H. Jansen, "The spectral-domain approach for microwave integral circuits," *IEEE Trans. Microwave Theory Tech.*, vol. MTT-33, pp. 1043–1056, Oct. 1985.
[19] K. C. Gupta, R. Garg, and R. Chadha, *Computer-Aided Design of Microwave Circuits*. Norwood, MA: Artech House, 1981, ch. 16–18.
[20] S. E. Davidson, S. A. Long, and W. F. Richards, "Dual band microstrip antenna with monolithic reactive loading," *Electron. Lett.*, vol. 26, pp. 936–937, 1985.
[21] J. R. James and P. H. Hall, *Handbook of Microstrip Antennas*, vol. I. London: Peter Peregrinus, 1989.
[22] J. C. Rautio and R. F. Harrington, "An electromagnetic time-harmonic analysis of shielded microstrip circuits," *IEEE Trans. Microwave Theory Tech.*, vol. MTT-35, pp. 726–730, Aug. 1987.
[23] G. V. Eleftheriades and J. R. Mosig, "On the network characterization of planar passive circuits using the method of moments," *IEEE Trans. Microwave Theory Tech.*, vol. 44, pp. 438–445, Mar. 1996.
[24] A. W. Glisson and D. R. Wilton, "Simple and efficient numerical methods for problems of electromagnetic radiation and scattering from

surfaces," *IEEE Trans. Antennas Propagat.*, vol. AP-28, pp. 593–603, Sept. 1980.
[25] T. W. Nuteson, K. Naishadham, and R. Mittra, "Spatial interpolation of the moment matrix in electromagnetic scattering and radiation problems," in *IEEE Antennas Propagat. Soc. Int. Symp. Dig.*, vol. 2, pp. 860–863, 1993.
[26] C. E. Baum, "The Singularity Expansion Method," in *Transient Electromagnetic Fields*, L. B. Felsen, Ed. New York: Springer-Verlag, 1976.
[27] D. C. Chang and J.-X. Zheng, "Electromagnetic modeling of passive circuit elements in MMIC," *IEEE Trans. Microwave Theory Tech.*, vol. 40, pp. 1741–1747, Sept. 1992.

Krishna Naishadham (S'83–M'87), for a photograph and biography, see this issue, p. 2173.

Pradeep Misra (S84–M'86), for a photograph and biography, see this issue, p. 2173.